DISSOLUTION AND MASS FLUX FROM TRICHLOROETHENE- AND TOLUENE-HEXADECANE MULTICOMPONENT NONAQUEOUS PHASE LIQUID (NAPL) MIXTURES

by

MARK CHRISTOPHER PADGETT

GEOFFERY R. TICK, COMMITTEE CHAIR
RONA J. DONAHOE
YUEHAN LU
KENNETH C. CARROLL

A THESIS

Submitted in partial fulfillment of the requirements
for the degree of Master of Science
in the Department of Geological Sciences
in the Graduate School of
The University of Alabama

TUSCALOOSA, ALABAMA

2015

ABSTRACT

Remediation efforts and contaminant transport predictions generally neglect the complicated dissolution and transport behavior associated with multi-component nonaqueous phase liquid (NAPL) sources. Therefore, it is important to understand the diffusion and dissolution processes occurring in these multicomponent systems as a function of mole fraction, molecular similarity/dissimilarity, and nonideal hydraulic factors. A series of laboratory scale NAPL-aqueous phase dissolution experiments were conducted to assess dissolution and intra-NAPL diffusion as a function of multicomponent NAPL composition (mole fraction) for both trichloroethene (TCE) and toluene (TOL). Predetermined volumes of target NAPL compounds were mixed with an insoluble n-hexadecane (HEX) NAPL to create mixtures that vary by NAPL composition. The ideality of resulting target compound dissolution was evaluated by quantifying NAPL-phase activity coefficient through Raoult's Law analysis. The results show that dissolution from the NAPL mixtures behave ideally for mole fractions above 0.2. As the target compound fraction of the NAPL mixture gets smaller, the dissolution behavior becomes increasingly nonideal (larger NAPL-phase activity coefficients). The TOL:HEX mole fraction mixtures show greater nonideality at equilibrium and initial elution concentrations for batch and column experiments when compared to TCE:HEX systems. Mass flux reduction analysis shows that the 0.5:0.5:, 0.2:0.8, and 0.1:0.9 mole fractions of both TCE and TOL behave similarly

while the 0.05:0.95 mole fractions of TCE and TOL behave the most nonideally and exhibit mass flux reduction before any other mole fractions. Overall, the dissolution rates were constant and not controlled by NAPL composition-dependent factors. The results of this work may be used to improve transport predictions, remediation design, and risk assessments especially for sites contaminated by complex NAPL mixtures.

LIST OF ABBREVATIONS AND SYMBOLS

C	Concentration
C_A	Dissolved phase concentration of component *I* from the NAPL mixture
Cm	Centimeter
C_S	Single component aqueous solubility
CTET	Carbon tetrachloride
DCE	Dichloroethene
DNAPL	Dense non-aqueous phase liquid
G	Gram
HEX	n-Hexadecane
I. D.	Inner diameter
J	Mass flux
K	Total number of components of a NAPL mixture
LNAPL	Light non-aqueous phase liquid
L	Liter
MFR	Mass flux reduction
Mg	Milligram
m_i	The moles of component (*i*) of the NAPL mixture

mL	Milliliter
m_T	The initial moles of all organic components in the NAPL mixture.
NAPL	Non-aqueous phase liquid
PCE	Tertachloroethylene
PV	Pore volume
Q	Volumetric flow rate
s	Seconds
TCE	Trichloroethylene
t_M	Intra-NAPL mass-transfer
TOL	Toluene
t_R	Relative residence time
UST	Underground storage tank
X_i^N	Mole fraction of component *i* in a NAPL mixture
γ_i^N	The activity coefficient of component *i* in the NAPL mixture which describes the effects of nonideal dissolution due to effects of a nonideal NAPL mixture

ACKNOWLEDGEMENTS

I want to give thanks to the many professors, friends, and faculty members who have helped me with this thesis. I especially want to thank Geoffrey Tick, the chairman of this thesis, for sharing his knowledge of NAPLs and contaminant transport processes over the past few years. I would also like to thank my committee members, Rona Donahoe, Kenneth C. Carroll, and Yuehan Lu for their valuable input. This research would not have been possible without the support of my fellow graduate students at The University of Alabama.

CONTENTS

ABSTRACT……...…… ii

LIST OF ABBREVIATIONS AND SYMBOLS…….. iv

ACKNOWLEDGEMENTS……...…… vi

LIST OF TABLES……..... ix

LIST OF FIGURES…… x

1. INTRODUCTION…….. 1

2. BACKGROUND…… 3

3. MATERIALS AND METHODS…… 7

3.1 MULTICOMPONENT SOLUTION PREPARATION……...…… 8

3.2 BATCH EXPERIMENTS…… 9

3.3 DYNAMIC COLUMN EXPERIMENTS…….. 10

4. RESULTS……. 13

4.1 BATCH EXPERIMENTS…….. 13

4.1.1 TOL:HEX STATIC BATCH EXPERIMENTS…….. 13

4.1.2 TCE:HEX STATIC BATCH EXPERIMENTS…….. 14

4.1.3 TOL:HEX TIME SERIES BATCH EXPERIMENTS…… 15

4.1.4 TCE:HEX TIME SERIES BATCH EXPERIMENTS…… 15

4.2 DYNAMIC FLOW (COLUMN) EXPERIMENTS…… 16

4.2.1 TOL:HEX AND SINGLE COMPONENT TOL SYSTEMS…….……...…….. 16

4.2.2 TCE:HEX AND SINGLE COMPONENT TCE SYSTEMS…….. 19

5. CONCLUSION……. 23

7. REFERENCES……. 26

LIST OF TABLES

1. Properties of the porous media (20/30-mesh Accusand) for column experiments…….. 29

2. Chemical Properties of relevant compounds……... 30

3. Experimental procedures for establishing NAPL and for dissolution flushing…..……. 31

4. TCE:HEX static batch results and predicted Raoult's Law values…….. 32

5. TOL:HEX static batch results and predicted Raoult's Law values..……... 33

6. Dissolution rates for the TCE:HEX and TOL:HEX multi-component NAPL mixtures……. 34

7. Activity coefficient values for both the batch and column Toluene experiments……... 35

8. Activity coefficient values for both the batch and column TCE experiments……. 36

LIST OF FIGURES

1. Schematic of Experimental Setup (adapted from Burke 2011)…… 37

2. Dissolution Rate calculation for the 0.5:0.5 TOL:HEX time series batch experiment……. 38

3. Dissolution Rate calculation for the 0.2:0.8 TOL:HEX time series batch experiment……. 39

4. Dissolution Rate calculation for the 0.1:0.9 TOL:HEX time series batch experiment……..... 40

5. Dissolution Rate calculation for the 0.05:0.095 TOL:HEX time series batch experiment….. 41

6. Dissolution Rate calculation for the 0.01:0.99 TOL:HEX time series batch experiment……. 42

7. Dissolution Rate calculation for the 0.5:0.5 TCE:HEX time series batch experiment……. 43

8. Dissolution Rate calculation for the 0.2:0.8 TCE:HEX time series batch experiment……. 44

9. Dissolution Rate calculation for the 0.1:0.9 TCE:HEX time series batch experiment……. 45

10. Dissolution Rate calculation for the 0.05:0.95 TCE:HEX time series batch experiment….. 46

11. Dissolution Rate calculation for the 0.01:0.99 TCE:HEX time series batch experiment….. 47

12. Toluene elution curves under uniformly packed conditions for differing mole fractions….. 48

13. Toluene mass flux reduction vs. fractional mass removed……. 49

14. TCE elution curves under uniformly packed conditions for differing mole fractions…… 50

15. TCE mass flux reduction vs. fractional mass removed……... 51

CHAPTER 1: INTRODUCTION

The contamination of soil and groundwater poses significant risk to human health and the environment through exposure from drinking water or ingestion. Hazardous waste sites are ubiquitous across the U.S. and characterization and remediation efforts are often complicated by the fact that they are contaminated by multiple chemicals and mixed-waste systems from multiple sources. Improper handling and disposal, spills, and leaking of underground storage tanks (UST) can also introduce dangerous chemicals into the environment, including both single and multi-component contaminant phases (Zhang et al., 2007). According to the USEPA, in 1991, 63% of hazardous waste sites surveyed reported detecting Non-Aqueous Phase Liquids (NAPLs) or NAPL-based constituents in monitoring wells, surface water, and/or soils (Haebeck, 1994). Various compounds, including light-NAPL (LNAPL) compounds such as hydrocarbon derivatives, dense-NAPL (DNAPL) compounds such as chlorinated solvents (TCE), and mixtures of the two can be found at hazardous waste sites and at many other contaminated sites across the country (Carroll and Brusseau, 2009; McCray and Brusseau, 1998; McCray and Dugan, 2002; Carroll et al., 2009; McCray et al., 2011). Included in these immiscible organic liquids (NAPLs) are petroleum fuels, chlorinated solvents, transmission oils, and coal tars. According to the National Research Council, the presence of immiscible liquids within the subsurface is the single most important factor limiting the cleanup of soil and groundwater

(NRC, 2005). Typically, NAPL dissolution is limited due to poor hydraulic accessibility and the very low aqueous solubility exhibited by specific NAPL compounds, making them extremely difficult to remove effectively via groundwater flushing (rate-limited dissolution processes). Multicomponent NAPL systems present further challenges for characterization and remediation because composition-dependent factors (changing mole fraction, molecular similarity/dissimilarity) will complicate dissolution processes compared to single-component NAPL systems. The aqueous solubility of the compounds in multicomponent NAPL systems can be reduced even more than in a single-component system providing a prolonged source-zone impact which may result in years or even decades of groundwater contamination (Brahma and Harmon, 2003; Zhang et al., 2007).

The purpose of this study is to evaluate the influence of target compound mole fraction and molecular structure on the dissolution behavior of two multicomponent NAPL systems; one which includes a target dense-NAPL (DNAPL) compound (TCE), and the other which includes a target light-NAPL (LNAPL) compound (TOL). The ideality of the dissolution processes is quantified through Raoult's Law analysis. Additionally, the removal effectiveness for each target compound mole fraction variant is evaluated through time-continuous reduction of mass flux during water flushing. A series of batch (equilibrium and time-series) and column experiments are conducted to determine the influence of intra-NAPL diffusion and aqueous dissolution of the target compounds within the multicomponent NAPL systems.

CHAPTER 2: BACKGROUND

NAPL mixtures or the diffusion of target NAPL compounds into a bulk NAPL can drastically change the dissolution and aqueous-phase mass transfer behavior of the overall system compared to that single component system. Therefore, the presence of a multicomponent NAPL system will further complicate the remediation process (McCray and Brusseau, 1998, 1999; Carroll and Brusseau, 2009). In fact, multicomponent NAPL systems are common and sites contaminated by only a single contaminant very seldom occur (Mercer and Cohen, 1990). The primary structure of these organic compounds are based on bonds of carbon and hydrogen atoms forming different chain lengths commonly associated with fossil fuels, crude oil, gasoline, coal, and natural gas (Schwartzenbach et al., 1993). Other types of chlorinated organic compounds such as tetrachloroethene (PCE), trichloroethene (TCE), dichloroethene (DCE), and carbon tetrachloride (CTET) are also prevalent at many contamination sites.

The dissolution behavior of multicomponent NAPL systems is complex and not thoroughly understood due to a variety of chemical properties and compositional effects present in such mixtures (Geller and Hunt, 1993; Carroll et al., 2009; Carroll and Brusseau, 2009). Understanding the dynamics and properties between each individual compound within a multicomponent system becomes increasingly important when the components have disparate properties or structural/molecular differences (aromatic vs. chained, differing solubility, etc.).

The degree of molecular similarity/dissimilarity as well as specific compound mole fraction may, in part, be responsible for observed nonideal dissolution behavior whereby resulting aqueous phase concentrations cannot be predicted using simplified equilibrium mass-transfer relationships (Raoult's Law). However, a form of Raoult's Law can be used to assess the degree of nonideal dissolution for such complex systems. Raoult's Law describes the equilibrium partitioning behavior between the components within the bulk NAPL and the aqueous phase as:

$$C_A = C_S x_i^N \gamma_i^N \qquad (1)$$

where C_A represents the dissolved phase concentration (amount in the dissolved phase) of component i from the NAPL mixture, x_i^N represents the mole fraction of component i in the NAPL mixture, C_S is the single-component aqueous solubility (maximum solubility in water) of component i of the NAPL mixture, and γ_i^N is the activity coefficient of component i in the NAPL mixture which describes the effects of nonideal dissolution due to effects of a nonideal NAPL mixture (molecular and compositional dissimilarity). The activity coefficient may be larger or smaller than unity when the components of the bulk NAPL are composed of different chemical compositions, sizes, shapes, and/or polarity characteristics. Moreover, it has been found that when the mole fraction is very small then the activity coefficient will likely deviate from unity (Banerjee, 1984; Burris and MacIntyre, 1985; Schwarzenbach et al., 1993, McCray and Dugan, 2002; Burke, 2011).

Previous experiments have tested impacts of nonuniform NAPL spatial distributions (NAPL "pools" or varying NAPL saturation with a column) on dissolution behavior (Zhang et al., 2007; Tick and Rincon, 2009; Burke, 2011). Hydraulic related factors such as bypass flow (NAPL-reduced permeability) and NAPL inaccessibility were shown to contribute to observed

nonideal dissolution behavior during flushing conditions. It is also expected that dissolution behavior will be impacted by the reduction of NAPL-water interfacial area as mass removal occurs during the flushing process (Burke, 2011). However, for multicomponent NAPL systems whereby a bulk of the NAPL is comprised of extremely low solubility (essentially insoluble) compounds, the bulk NAPL-water interfacial area should remain constant as dissolution progresses. Under such circumstances, dissolution behavior should primarily be influenced by hydraulic related factors, compositional-dependent factors, and chemical/molecular structure differences within the bulk NAPL mixture.

A common approach to evaluate the effectiveness of mass removal as a function of the NAPL dissolution process is through the analysis of time-continuous mass flux reduction during aqueous flushing conditions (Carroll and Brusseau, 2009; DiFilippo et al., 2010; Tick and Rincon, 2009). Such analyses can provide insight into the physical heterogeneity of the system, the distribution of the NAPL source (uniform vs. nonuniform or NAPL architecture), and the specific NAPL compounds experiencing limited removal for a multicomponent system. Instead of only relying on aqueous concentration-based assessments of removal effectiveness, mass flux reduction analyses provide a means to evaluate impacts from the processes mentioned above (Soga et al., 2004). Time-continuous mass flux reduction (MFR) analysis compares the rate of mass flux reduction to the total mass of contaminant removed from the system and is defined as:

$$MFR = 1 - \frac{J_f}{J_i} = 1 - \frac{Q_f C_f}{Q_i C_i} \qquad (2)$$

where J is the mass flux (M/AreaTime^{-1}), Q is the volumetric flow rate (L^{3}T^{-1}), C is concentration (ML^{-3}), and the subscripts i and f represent initial and final, respectively. If flow rate is held constant then the prior equation reduces to:

$$MFR = 1 - \frac{C_f}{C_i} \tag{3}$$

Ideal or efficient mass removal occurs when maximum mass flux (dissolution rate) is maintained over a time period whereby most of the contaminant mass in the system is removed. In such systems it is expected NAPL-water interfacial area is maximized (uniform distributions within homogeneous media) and high aqueous solubility compounds are most present and not likely subject to major rate-limitations due to disparate NAPL compositional related factors. In contrast, nonideal or inefficient mass removal occurs when contaminant mass flux is reduced significantly while a majority of the mass still remains in the system. This behavior leads to prolonged flushing with negligible or limited contaminant mass removal over time. Such systems are influenced by nonuniform NAPL distributions (pools) or hydraulically inaccessible mass (limited NAPL-water interfacial area) related to porous media heterogeneity, low aqueous solubility compounds, or significant compositional differences of components within complex NAPL mixtures.

CHAPTER 3: MATERIALS AND METHODS

Physical properties of all three NAPL compounds and the porous medium can be found in Tables 1 and 2. Analytical grade TCE (>99.5% purity) was purchased from Sigma-Aldrich Chemical and Toluene (TOL) (99.9% purity) was purchased from Fisher Scientific. These compounds were selected as representative contaminants as they are common components of NAPL mixtures and they define both classes of NAPL (dense-NAPL and light-NAPL). The insoluble NAPL n-Hexadecane (HEX) (>99% purity) was purchased from Alpha-Aesar. N-Hexadecane was chosen to reduce the number of variables (decrease in interfacial area) contributing to dissolution. The insoluble nature will tend to keep the bulk NAPL volume and interfacial area constant through time of flushing. The porous medium used in column experiments was a homogeneous 20/30-mesh quartz Accusand© (Unimin Corp., Le Seur, MN, USA). The porous medium has a porosity of 32% and a bulk density of 1.78 $g \cdot cm^{-3}$, and an intrinsic permeability of 1.38×10^{-10} cm^2. Other properties for the porous media are listed in Table 1. The column itself was made of stainless steel (2.2 cm I.D., 7-cm length, Alltech Co.) and re-used for each column experiment. The column was designed to have little void space in each of the ends and was fitted with 1-inch Opti-flow fittings. Airtight glass syringes (Popper & Sons, Inc. New Hyde Park, New York, USA) were used to sample in both the column and batch experiments. Twenty milliliter (mL) vials from VWR were used, along with Sun-Sri crimp caps,

during the static and time series batch experiments in order to store the samples in airtight containers. The flushing solution used for the column experiments was a 0.01 N $CaCl_2$ synthetic groundwater solution.

3.1 Multi-component Solution Preparation

The multicomponent NAPL mixtures were prepared as ratios for both TCE:HEX and TOL:HEX bulk NAPLs which included mole fractions of 0.5:0.5, 0.2:0.8, 0.1:0.9, 0.05:0.95, and 0.01:0.99, respectively. The following equation was used to calculate mole fractions for each particular bulk NAPL system:

$$X_i = \frac{m_i}{\sum_{i=1}^{k} m_i} \quad \text{or, alternatively as:} \quad X_i = \frac{m_i}{m_T} \qquad (4)$$

where X_i is the mole fraction of component (i) of the NAPL mixture, k is the total number of components in the NAPL mixture, m_i are the moles of component (i) of the NAPL mixture, and m_T is the initial moles of all organic components in the NAPL mixture.

Each NAPL mixture was prepared in 100 mL volumetric flasks (filled to top with no head space) in order to ensure each system was homogenous and uniform for each of the experiments. Thus, most volumetric flasks averaged a total volume around 106 mL. First, the volume fraction (measured by glass syringe) of TOL or TCE required to obtain the desired mole fraction was added to the container. Last, n-Hexadecane was added to the container until no headspace was left in the volumetric flask. After the flask was full, the borosilicate top was positioned and sealed with Parafilm to ensure no volatilization would take place. After the solution was mixed, it was put on a Barnstead-Labline A-Class shaker table for a period of 4 days to ensure adequate homogenization of the two-component (TOL:HEX or TCE:HEX) NAPL system. All experiments that utilized multicomponent NAPL mixtures were consistently

prepared using this method. If excess was present after the vials had been opened, the excess was discarded due to the effect volatilization might have on the volume/mole fraction accuracy.

3.2 Batch Experiments

The first set of experiments sought to determine how differing mole fractions affected the dissolution behavior of the multi-component NAPL mixtures under static, equilibrium conditions. A series of 20-mL headspace vials were arranged for a time series evaluation over a 72-hour period. Each series contained 10 vials to be tested at specific time intervals. NAPL mixture preparation was the same as outlined in the above section. After the multicomponent NAPL was prepared, a 10 mL sample was placed in contact with 10 mL Nano-pure water in a 20-mL vial and crimp-sealed with Teflon septa and aluminum caps so that no headspace was present. Ten milliliter pipettes were used to emplace the Nano-pure water and 10-mL glass syringes were used to emplace the NAPL phase. The initial fluid placed in the vial was chosen based on the particular NAPL density. The denser-than-water NAPL (DNAPL) phase was placed in the vial first in order to avoid fluids passing through each other upon placement. The Nano-pure water phase was then added on top. For the LNAPL phase, the Nano-pure water was placed first in the vial followed by the bulk LNAPL. For a DNAPL, the NAPL was placed in the vial first then water was added on top. The vials were then crimp-sealed ensuring that the system had no headspace and volatilization could not occur. No shaking or stirring occurred in order to keep the system static.

The first sample was taken one hour after the NAPL was placed in contact with the water. Subsequent samples were taken at 2, 4, 6, 8, 12, 16, and 24 hours after NAPL-water interaction was initiated. Two additional samples were taken after 48 and 72 hours of NAPL-water contact in order to ensure equilibrium conditions had been achieved. Aqueous phase subsamples were

collected and from the headspace vials via a glass syringe in order to determine concentration-time relationships. Due to density differences, the sampling method also differed between LNAPL and DNAPL samples. For a DNAPL solution, the aqueous sample could simply be taken from the top of the vial, as the water was present above the DNAPL. For a LNAPL, the use of a stainless steel hypodermic needle (10.2 cm) was attached to the glass syringe in order to reach the aqueous phase below the LNAPL. Subsamples were transferred to 10-mL volumetric flasks (diluted if necessary) and analyzed immediately for TCE or TOL after being removed from the vial in order to ensure minimal loss due to volatilization. Duplicate samples were taken to ensure analytical consistency. For both static and time-series batch experiments, each vial was sacrificed after each subsample was collected for analysis. Samples were analyzed using a UV-Vis spectrophotometer (Shimadzu UV-1700) with a detection limit of 0.1 $mg \cdot L^{-1}$.

3.3 Dynamic Column Experiments

A series of column experiments were conducted to investigate the effects of varying NAPL-phase mole fraction (TOL:HEX and TCE:HEX) on dissolution behavior during water flushing conditions. Ten different column systems were designed to test each differing mole fraction of TCE and TOL (5 mole fractions for TCE:HEX and TOL:HEX). Two additional column experiments tested single-component pure-phase TCE and TOL dissolution behavior for comparison to the multicomponent systems. Prior to the establishment of the multicomponent NAPL residual saturation and the initiation of the dissolution experiments (range of mole fractions), the respective target NAPL component (TCE or TOL) was mixed with insoluble HEX to create a bulk NAPL mixture at a desired mole fraction. The “insoluble” pure-phase HEX was chosen so that the distribution and NAPL-water interfacial would remain constant throughout the duration of the dissolution experiments.

Columns were packed incrementally (0.5-cm increments) with a dry quartz-sand Accusand (20/30 mesh size) to create physically homogeneous and uniform porous medium systems. Conservative tracer tests were conducted within such porous media systems to provide further confidence that the systems were packed uniformly and that conditions were advection dominated (Peclet numbers of 80-110 based on Burke, 2011). Once the columns were completely packed with sand, the column end-fittings were then secured. The top end fitting included a polyethylene screen (0.2-mm pore openings) as well as dispersion frit to ensure homogeneous flow throughout the column. The bottom end fitting of the column contained a single screen mesh in order to contain the sand within the column. The columns were then saturated with Nano-pure water for approximately 48-hours from the bottom up using an HPLC piston pump (Lab Alliance, Acuflow Series I). Once the column weight stabilized for at least 12 hours after the initial 48-hour saturation period, the saturation process was ceased and the columns were sealed. This saturation processes allowed for the gravimetric quantification of the pore volume (PV) and the porosity for each column system prior to NAPL imbibition and dissolution flushing.

Following aqueous saturation, the columns were imbibed with the bulk-NAPL to establish residual saturation using the similar methods described by Pennell et al. (1993), Bai et al. (1997), and Boving and Brusseau (2000). The particular mole-fraction NAPL (TCE:HEX or TOL:HEX) or single-component NAPL (TCE or TOL) was injected vertically into the packed column (from top or bottom) using a syringe pump (KD Scientific Model 780100) and gas-tight glass syringe depending on the density of the bulk-NAPL to ensure stable displacement conditions. For an LNAPL system injection was downward and for a DNAPL system injection was upward (Table 3). In all cases, the NAPL was imbibed at an injection rate of 0.2 $mL \cdot min^{-1}$.

Residual NAPL saturation conditions were established in 2 sequential flushing steps: 1) pumping TCE- or TOL-saturated (aqueous solubility) solutions at a rate of 8.5 $cm \cdot hr^{-1}$ for 2 PVs; and 2) then followed by 10 PVs of flushing at a flow rate of 85 $cm \cdot hr^{-1}$. The vertical direction of these aqueous flushing steps was dependent of NAPL density in order to maintain stable displacement conditions (Table 3). The amount of NAPL within each system was determined volumetrically by measuring the amount of NAPL that remained in the column after injection and establishment of residual saturation conditions. Initial NAPL saturations (S_N) were targeted at 20% for all dissolution flushing experiments (Table 3). Once initial saturations were established, the aqueous phase flushing (dissolution experiments) began and effluent concentrations were monitored for the duration of the experiment.

All dissolution experiments were conducted under stable displacement conditions and were conducted using 0.01 N $CaCl_2$ synthetic groundwater in order to simulate groundwater flow conditions. Samples were collected using a gas-tight glass syringe and placed into 10-mL volumetric flask for analysis in the same manner described previously (batch experiments). TCE or TOL samples were collected to generate full elution curve profiles and the dissolution experiments were terminated once significant low-concentration tailing conditions occurred. An example of the schematic setup is shown in Figure 1.

CHAPTER 4: RESULTS AND DISCUSSION

The results of 10 static batch experiments, 10 time-series batch experiments, and 10 column experiments are presented. Specifically, this included experiments for various mole fractions of the multicomponent NAPL mixtures (TCE:HEX and TOL:HEX) as well as the additional single-component NAPL (TCE and TOL) set of experiments. The single-component column experiments provided a means for comparing initial dissolution behavior to that of the multicomponent systems.

4.1 Batch Experiments

4.1.1 TOL:HEX Static Batch Experiments

These series of batch experiments were conducted to evaluate equilibrium dissolution behavior for the specific multicomponent (mole fractions) NAPL mixtures. Final aqueous phase TOL concentrations (72-hour equilibration) were measured and compared to Raoult's Law predictions. Maximum TOL solubility was achieved around 24 hours into the experiment for each mole fraction tested. As expected, final equilibrium aqueous concentrations decreased as a function of decreasing initial TOL mole fraction. However, the equilibrium aqueous TOL concentrations (72-hour equilibration) could not be predicted using Raoult's Law with NAPL-phase activity coefficients (γ_i^N) close to unity (Schwarzenbach, et al., 1993; McCray and

Brusseau, 1998). For example, Raoult's Law under-predicted TOL concentrations by a factors of almost 3 to 9 for decreasing TOL mole fractions (TOL:HEX mole fraction ratios 0.1:0.9, 0.05:0.95, and 0.01:0.99), respectively. In fact, there was a clear trend of increasing nonideal dissolution behavior with decreasing TOL mole fraction for the TOL:HEX system (Table 4). This can be observed from the progressively increasing γ_i^N values with decreasing TOL mole fraction. Similarly, this indicates that the NAPL mixtures were progressively more nonideal as TOL mole fraction decreased. Equilibrium TOL dissolution showed notable differences in behavior compared to the TCE equilibrium batch experiments (Tables 4 and 5). This may suggest that molecular structure differences between TOL and TCE within a bulk NAPL which will result in variable dissolution behavior that may lead to erroneous aqueous-phase concentration predictions in groundwater using common Raoult's Law approaches. Fitting TOL concentrations through adjustment of γ_i^N values indicates that TOL experiences greater molecular dissimilarity (with respect to the bulk NAPL, Hexadecane) than TCE (*following section 4.1.2*). Such molecular differences may be a result of greater variation between the aromatic structure of TOL and the aliphatic structure of HEX compared to TCE (aliphatic).

4.1.2 TCE:HEX Static Batch Experiments

Maximum TCE solubility was achieved around 24 hours into the experiment for each mole fraction tested. As expected, final equilibrium aqueous concentrations decreased as a function of decreasing initial TCE mole fraction. Overall, TCE concentrations were consistent with Raoult's Law predictions whereby concentrations could be predicted with NAPL-activity coefficients (γ_i^N) close to that of unity (calculated values between 1.02 and 1.84 for all mole fractions) (Table 5). NAPL-activity coefficient values ranging between 1 and 2 generally describe ideal NAPL mixtures whereby Raoult's Law can be applied (Schwarzenbach, et. al.,

1993; McCray and Brusseau, 1998). This suggests that the multicomponent NAPL (TCE:HEX) mixtures and resulting dissolution processes were relatively ideal for the conditions of these experiments. This may be a result of greater chemical/molecular similarity between the aliphatic structure of TCE and the aliphatic structure of HEX compared to TOL (aromatic).

4.1.3 TOL:HEX Time-Series Batch Experiments

Time-series batch experiments were conducted to determine dissolution rates and evaluate effects of rate-limited intra-NAPL diffusion for the range of TOL:HEX NAPL mole fractions. Dissolution rates were determined by the slope of the relative concentration vs. time plots (Table 6) (Figures 2-6). Dissolution rates were consistent (varying by a factor if 0.3; avg. = 2.8×10^{-5} s^{-1}) independent of the particular mole fraction tested. Overall, the variance for the dissolution rates was 1.7×10^{-10}, indicating similar time-dependent dissolution behavior for all mole-fraction systems. For this reason and because there was no observed trend of dissolution rate with TOL:HEX NAPL mole fraction, it is concluded that rate-limited intra-NAPL diffusion processes were likely negligible under these conditions.

4.1.4 TCE:HEX Time-Series Batch Experiments

Dissolution rates for the various TCE:HEX mole fraction NAPL systems were less consistent compared to the TOL:HEX systems, varying within an order of magnitude (~1-3 ×) of each other (avg. = 1.98×10^{-5} s^{-1}) (Table 6). Figures 7-11 show the graphs of relative concentration vs. time that were used to calculate the dissolution rates for each mole fraction. Overall, the variance for the dissolution rates was 5.52×10^{-11}, approximately one order of magnitude smaller than the TOL:HEX systems. Furthermore, a noticeable positive linear trend (R^2=0.71) of dissolution rate with TCE:HEX NAPL mole fraction was observed. This suggests that mass transfer (dissolution) rates are dependent on the initial mass of target component (TCE)

and that rate-limited intra-NAPL diffusion effects may have been acting in these systems. The different time-series dissolution behaviors observed between TCE and TOL may be a result of molecular dissimilarity (contrast) effects (mixture nonideality) within the bulk NAPL (HEX).

4.2 Dynamic Flow (Column) Experiments

Ten column experiments were conducted to determine the dissolution behavior for four mole fractions of TOL:HEX and TCE:HEX multicomponent NAPL systems and single-component NAPL systems (TOL and TCE) under dynamic flow conditions. Aqueous-phase elution curves for the target component (TOL or TCE) were used to evaluate dissolution behavior and mass flux reduction during the period of water flushing. As mentioned previously, "insoluble" pure-phase HEX was chosen as the bulk NAPL for the multicomponent NAPL systems so that the distribution and NAPL-water interfacial would remain constant throughout the duration of the dissolution experiments. Therefore, elution (dissolution) behavior would be expected to independent of NAPL interfacial area reduction over time (unlike the single-component systems).

4.2.1 TOL:HEX and Single-Component TOL Systems

The multicomponent systems experienced much shorter steady-state elution periods than the single-component TOL dissolution experiments. For the multicomponent systems, the steady-state elution lasted between 30-70 PVs (~5× shorter than single-component TOL experiments) demonstrating that each mole fraction could maintain a period of equilibrium dissolution (Figure 12). After the period of steady-state dissolution, the rate of concentration decrease (transient-state) was different for each NAPL mole-fraction system tested. Such behavior may be due to rate-limited intra-NAPL diffusion, differences in NAPL distribution and saturation within the column, and/or hydraulic-related factors such as bypass flow. For the

0.5:0.5, 0.2:0.8, and 0.1:0.9 TOL:HEX mole fraction systems the rate of dissolution decrease (albeit different for each respective system) was relatively constant without a significant tailing stage, indicating that sufficient NAPL-water interfacial area (assumed constant) may have been maintained allowing for mass-transfer rates to be relatively constant over the duration of flushing. Additionally, the observed higher rate of transient-state concentration decline for the 0.5:0.5 TOL:HEX system may have also been influenced by a reduction in total NAPL interfacial area (and volume), as a significant portion of the NAPL bulk phase would be depleted as the more soluble target compound (TOL) was removed via dissolution processes. The 0.05:0.95 TOL:HEX system showed pronounced tailing after about 100 PVs of flushing, indicating that the relatively low TOL mass within the NAPL may have been subject to greater intra-NAPL mass-transfer (t_M) limitations and/or relative residence time (t_R) effects ($t_R > t_M$). The single-component TOL dissolution experiment resulted in steady-state elution behavior for 230 PVs, followed by a rapid decline in concentration until tailing occurred after about 370 PVs of water flushing. The primary tailing behavior was likely due to a significant reduction in TOL (NAPL) mass and NAPL-water interfacial area.

Steady-state elution concentrations were higher than that predicted by the "ideal" form Raoult's Law ($\gamma_i^N \approx 1$) for the TOL:HEX NAPL systems. In order to evaluate system dissolution nonideality, Raoult's Law was used to match observed initial maximum steady-state elution concentrations through adjustment (fitting) of the NAPL-phase activity coefficient (γ_i^N) (Table 7). For the TOL:HEX systems, activity coefficient values increased slightly (1.5-2.3) as a function of decreasing initial TOL mole fraction, exhibiting a similar trend to that observed for the batch experiments. Under such conditions, these systems behaved relatively ideal during the initial phases of flushing. However, the calculated activity coefficients were slightly smaller

compared to those determined from the batch experiments and is likely a result of nonideal hydraulic related factors such as NAPL bypass flow, permeability variations, and/or variations in mass-transfer and residence times. The single-component TOL dissolution experiment resulted in initial steady-state concentrations (avg. = 580 $mg \cdot L^{-1}$) that were approximately consistent to the aqueous solubility limit of TOL (~535 $mg \cdot L^{-1}$). As expected, initial steady-state concentrations could be predicted using the "ideal" form of Raoult's Law ($\gamma_i^N \approx 1$).

Time-continuous mass flux reduction (MFR) analyses were used to evaluate the efficiency of contaminant removal processes. The most efficient (ideal) removal process is described by conditions whereby minimal MFR (maximum mass flux) occurs until nearly all of the mass in the system is removed. MFR behavior varied significantly depending on the specific initial TOL mole fraction (TOL:HEX NAPL system) (Figure 13). In general, longer maximum steady-state TOL mass flux (more ideal removal) occurred as a function of higher initial TOL mole fractions. For instance, TOL:HEX initial mole fraction systems of 0.5:0.5, 0.2:0.8, 0.1:0.9, and 0.05:0.95 maintained maximum (mass flux) TOL removal for conditions by which approximately 36, 18, 14, and 6% of the total mass in the systems was removed, respectively.

The steady-state maximum mass flux (low MFR) was followed by a transient MFR period (slow removal phase) until nearly all of the mass was removed from the system. The rate of transient MFR was similar (relatively constant) for the initial 0.2 and 0.1 TOL mole fraction systems. Interestingly, the 0.5:0.5 TOL:HEX system exhibited more nonideal (inefficient) TOL removal after the initial steady-state removal phase at which point MFR occurred drastically until nearly complete mass removal was achieved. This behavior may be due to a more significant reduction in NAPL volume (NAPL-water interfacial area) as the greater fraction of "soluble" target component (TOL) was removed compared to the other TOL:HEX systems.

Thus, higher TOL mole fraction systems (≥ 0.5) may be more sensitive to later-time removal as the reduction in NAPL source interfacial area plays a more dominant role on resulting dissolution and MFR, contributing to overall less ideal removal behavior. The least ideal mass removal was observed by the 0.05:0.95 TOL:HEX mole fraction system as it exhibited a very short maximum mass flux period followed by a rapid transient-state MFR phase until near complete mass removal was achieved. This nonideal removal behavior was most likely due to the extremely small amount of TOL within the initial mole fraction NAPL system whereby rate-limited intra-NAPL diffusion, mixture nonideality, mass transfer vs. residence time, and dilution effects may exhibit a relative stronger influence on resulting flushing/removal processes.

The single-component TOL flush exhibited relatively ideal removal behavior in terms of MFR analysis. This more ideal removal behavior is a result of the significant TOL mass in the system, providing the conditions for maximum mass flux (dissolution) to occur over the entirety of flushing period. Maximum mass flux (low MFR) was maintained for a longer period of TOL mass removal (~50-80%) before significant transient-state MFR occurred until near complete mass removal was achieved.

4.2.2 TCE:HEX and Single-Component TCE Systems

Similar to the TOL column experiments, the multicomponent TCE:HEX systems exhibited much shorter steady-state elution times than the single-component TCE dissolution experiments (Figure 14). For the multicomponent systems, the steady-state elution lasted between 3-50 PVs (~2-3× shorter than single-component TCE experiments). All TCE:HEX initial mole fraction systems supported a period of equilibrium dissolution, with the exception of the 0.05:0.95 TCE:HEX mole fraction system whereby a nearly immediate decline in TCE concentration occurred soon after flushing was initiated. This indicates that, for the 0.05:0.95

TCE:HEX system, the low initial TCE mass present was not sufficient to maintain any period of steady-state dissolution. After the period of steady-state dissolution, the rate of concentration decrease (transient-state) was slightly different for each NAPL mole-fraction system tested. Such behavior may due to nonideal hydraulic-related and rate-limited mass transfer processes as described in the previous section (*section 4.2.1*). For all TCE:HEX mole fraction ranges, the rate of dissolution decrease (albeit different for each respective system) was relatively constant without a significant tailing stage, indicating that sufficient NAPL-water interfacial area (assumed constant) may have been maintained allowing for mass-transfer rates to be relatively constant over the duration of flushing. The single-component TCE dissolution experiment resulted in steady-state elution behavior for 100 PVs, followed by a relatively rapid decline in concentration until tailing occurred at about 150 PVs of water flushing. The primary transient phase elution and tailing behavior was likely due to a reduction in TCE (NAPL) mass and NAPL-water interfacial area as flushing progressed.

Steady-state elution concentrations were slightly higher than that predicted by the "ideal" from Raoult's Law ($\gamma_i^N \approx 1$) for the TCE:HEX NAPL systems. Initial TCE elution concentrations were matched by fitting NAPL-water activity coefficients (1.24-3.97) for the column experiments. For the 0.5:0.5, 0.2:0.8, and 0.1:0.9 TCE:HEX mole fraction systems, elution concentrations could be predicted well using Raoult's Law ($\gamma_i^N \approx 1$, avg. = 1.3) and there was no particular trend observed for γ_i^N as a function of mole fraction. However, a greater value of γ_i^N was required to match the initial elution concentration for the low TCE mole fraction system (0.05:0.95 TCE:HEX). Therefore, when the target component mole fraction (TCE) is smaller than some critical value, dissolution and aqueous phase concentrations likely cannot be predicted with the "ideal" form of Raoult's Law. The anomalous dissolution behavior for such

multicomponent NAPL systems will likely be influenced by NAPL-mixture nonideality. The single-component TCE dissolution experiment resulted in initial steady-state concentrations (avg. = 1,250 $mg \cdot L^{-1}$) that were consistent to the aqueous solubility limit of TOL (~1,200 $mg \cdot L^{-1}$). As expected, initial steady-state concentrations could be predicted using the "ideal" form of Raoult's Law ($\gamma_i^N \approx 1$).

Time-continuous MFR behavior varied depending on the specific initial TCE mole fraction (TCE:HEX NAPL system). With the exception of the lowest TCE mole fraction (0.05:0.95 TCE:HEX), all other TCE:HEX mole fraction systems maintained an initial period whereby maximum steady-state mass flux (most ideal removal conditions) occurred up to approximately 40-50% mass removal (Figure 15). This initial steady-state removal behavior was generally more ideal (efficient) than the TOL:HEX initial removal conditions and may be related to the higher aqueous solubility of TCE and/or variations in porous media packing and NAPL saturation/distribution. However, similar to the low TOL mole fraction (0.05:0.95 TOL:HEX) system, the 0.05:0.95 TCE:HEX lacked any notable maximum mass flux period whereby MFR occurred immediately upon aqueous flushing until nearly all the mass was removed (least ideal mass removal-inefficient).

The steady-state maximum mass flux (low MFR) was followed by a transient MFR period (slow removal phase) until nearly all of the mass was removed from the system. The rate of transient MFR was nearly identical (relatively constant) for all multicomponent TCE:HEX systems except the lowest 0.05:0.95 TCE:HEX mole fraction system. The 0.5:0.5 TCE:HEX system may have exhibited slightly less ideal (inefficient) removal than the 0.2 and 0.1 TCE mole fraction systems which may be due to a greater reduction in NAPL volume (NAPL-water interfacial area) as described for 0.5:0.5 TOL:HEX system. The least ideal mass removal was

observed by the 0.05:0.95 TCE:HEX mole fraction system which immediately experienced MFR with initiation of water flushing conditions. This nonideal removal behavior was most likely due to the extremely small amount of TCE within the initial mole fraction NAPL system whereby rate-limited intra-NAPL diffusion, mass transfer vs. residence time, and dilution effects may exhibit a relative stronger influence on resulting flushing/removal processes. These trends are supported by previous batch experiments conducted within this study.

The single-component TCE flush exhibited relatively ideal removal behavior in terms of MFR analysis. This more ideal removal behavior is a result of the significant TCE mass in the system, providing the conditions for maximum mass flux (dissolution) to occur over the entirety of flushing period. Maximum mass flux (low MFR) was maintained for a longer period of TOL mass removal (~60%) before significant transient-state MFR occurred until near complete mass removal was achieved.

CHAPTER 5: CONCLUSION

This study demonstrated that across most mole fractions, TCE exhibited relatively ideal dissolution behavior from a bulk HEX NAPL whereby Raoult's Law could be used to predict equilibrium and initial aqueous TCE concentrations during batch and column experiments, respectively. NAPL-phase activity coefficient values, which ranged from 1-2, were effectively independent of mole fraction. However, the lowest TCE mole fractions exhibited nonideal dissolution behavior (NAPL mixture nonideality) whereby Raoult's Law could not be used for prediction. This suggests that as the target compounds mole fraction decreases within a NAPL mixture, dissolution processes cannot be described using equilibrium relationships and that rate-limited intra-NAPL diffusion, dissolution, and/or molecular dissimilarity impose greater control on mass transfer. Dissolution behavior for all TOL:HEX mole fraction mixtures showed overall greater degrees of nonideality for equilibrium and initial elution concentrations for batch and column experiments, respectively, compared to TCE:HEX systems. Similar to TCE:HEX experiments, it was observed that greater dissolution nonideality occurred with lower TOL mole fraction in the NAPL mixture. Dissolution rates for the TCE:HEX (DNAPL) and TOL:HEX (LNAPL) systems were relatively consistent in magnitude. Dissolution rates for the TOL:HEX systems were shown to be independent of TOL mole fraction. However, dissolution rates for the TCE:HEX multicomponent systems showed a positive correlation with initial TCE mole fraction

indicating that rate-limited intra-NAPL diffusion effects may have been rate-limiting in these systems. Mass flux reduction analysis demonstrated that more ideal (i.e., efficient) mass removal conditions occurred for TCE compared to TOL during multicomponent water flushing. In general, TCE experienced more ideal dissolution and mass removal conditions which may be a result of greater molecular similarity (mixture ideality) and/or solubility effects within the bulk NAPL (HEX) compared to that of toluene (TOL). Appropriate characterization of NAPL mixtures is required to effectively predict the resulting aqueous phase concentrations allowing for more accurate risk assessments and contaminant transport predictions, and the development of more effective remediation strategies.

REFERENCES

Bai, M., Elsworth, D., Inyang, H. I., and Roegiers, J.C., 1997. Modeling contaminant migration with linear sorption in strongly heterogeneous media. Journal of Environmental Engineering, 123(11):1116-1125

Banerjee, S., 1984, Solubility of organic mixtures in Water, Environmental Science Technology. 18 (8), 587-597

Boving, T.B., and Brusseau, M.L. 2000. Solubilization and removal of residual Trichloroethene from porous media: Comparison of several solubilization agents. Journal of Contaminant. Hydrology., 42, 51-67.

Brahma, P.P. and Harmon, T.C., 2003. The effect of multi-component diffusion on NAPL dissolution from spherical ternary mixtures. Journal of Contaminant Hydrology, 67(1-4):43-60

Burke, W.R., 2011. Rate Limited Diffusion and Dissolution of Multi-Component Non-Aqueous Phase Liquids (NAPLs). Thesis

Burris, D.R., and W.G. MacIntyre, 1985. Water solubility behavior of binary hydrocarbon mixtures, Environ. Toxicol. Chem., 4, 371– 377

Carroll, K.C., 2007. Characterization, Dissolution, and Enhanced Solubilization of Multi-component Non-Aqueous Phase Liquid in Porous Media. A Dissertation Submitted to the Faculty of the Department of Hydrology and Water Resources, University of Arizona

Carroll, K.C., and Brusseau, M.L., 2009. Dissolution, cyclodextrin-enhanced solubilization, and mass removal of an ideal multicomponent organic liquid. Journal of Contaminant Hydrology. 106, 62-72.

Carroll, K.C., Taylor, R., Gray, E., and Brusseau, M.L., 2009. The impact of composition on the physical properties and evaporative mass transfer of a PCE-diesel immiscible liquid. Journal of Hazardous Materials. 164, 1074-1081.

DiFilippo, E.L., Carroll, K.C., and Brusseau, M.L., 2010. Impact of organic-liquid distribution and flow-field heterogeneity on reductions in mass flux. Journal of Contaminant Hydrology. 115, 14-25

Geller, J.T., and Hunt, J.R., 1993. Mass transfer from nonaqueous phase organic liquids in -saturated porous media. Resources Research, 29(4), 833-845

Haebeck, M., 1994. Toxicological Profile for Toluene. Agency for Toxic Substances and Disease Registry: United States Public Health Service

McCray, J.E., and Brusseau, M.L., 1998, Cyclodextrin-Enhanced in Situ Flushing of Multiple-Component Immiscible Organic Liquid Contamination at the Field Scale: Mass Removal Effectiveness. Environ. Sci. Technol., 32(9), 1285-1293

McCray, J.E., and M.L. Brusseau, 1999. Enhanced in-situ flushing of multiple component immiscible organic liquid contamination at the field scale using cyclodextrin: Mass-transfer phenomena, Environ. Sci. Technol., 33(1), 89– 95.

McCray, J.E., and Dugan P.J., 2002, Non-ideal equilibrium dissolution of trichloroethene from a decane-based nonaqueous phase liquid mixture: Experimental and modeling investigation. WATER RESOURCES RESEARCH, VOL. 38, NO. 7, 1097

McCray, J.E., Tick, G.R., Jawitz, J.W., Gierke, J.S., Brusseau, M.L., Falta, R.W., Knox, R.C., Sabatini, D.A., Annable, M.D., Harwell, J.H., and Wood, A.L., 2011. Remediation of NAPL Source Zones: Lessons Learned from Field Studies at Hill and Dover AFB. Ground Water, 49(5), 727-744

Mercer, J.W., and Cohen, R.M. 1990. A review of immiscible fluids in the subsurface: Properties, models, characterization and remediation. J. Contam. Hydrol., 54, 174-193.

National Research Council (NRC) (U.S.). 1999. Groundwater and Soil Cleanup: Improving Management of Persistent Contaminants. Washington, DC: National Academy of Sciences.

National Research Council (NRC) (U.S.). 2000. Research Needs in Subsurface Science. Washington, DC: National Academy of Sciences

Pennell, K.D., Abriola, L.M., and Weber, W.J. 1993. Surfactant enhanced solubilization of residual dodecane in soil columns. 1. Experimental investigation. Environ. Sci. Technol., 27(12), 2332–2340

Schwartz, F.W., and Zhang, H., 2003. Fundamentals of ground water, John Wiley & Sons, New York, NY, United States, 583

Schwarzenbach, R.P., Gschwend, P.M., and Imboden, D.M., 1993. Environmental Organic Chemistry, Wiley Interscience, New York

Soga, K., Page, J.W.E., and Illangasekare, T.H. 2004. A review of NAPL source zone remediation efficiency and the mass flux approach. J. Hazard. Mater., 110(1–3), 13–27

Tick, G.R., and Rincon, E., 2009. Effect of enhanced-solubilization agents on dissolution and mass flux from uniformly distributed immiscible liquid trichloroethene (TCE) in homogeneous porous media. Water, Air, and Soil Pollution. 1.1001/s11270-009-0047-3

Wilson, W.E., and Moore, J.E. 1998. American Geological Institute: Glossary of Hydrology, American Geological Institute, Alexandria, VA.

Zhang, Z., and Brusseau, M.L., 1999. Non-ideal transport of reactive solutes in heterogeneous porous media 5. Simulating regional-scale behavior of a trichloroethene plume during pump and-treat remediation. Water Resources Research. Vol. 35(10), 2921-2935.

Zhang, C., Werth, C.J., and Webb, A.G., 2007. Characterization of NAPL source zone architecture and dissolution kinetics in heterogeneous porous media using magnetic resonance imaging. Environmental Science Technology, 41, 3672-3678

Property	Value
*Uniformity coefficient (d_{60}/d_{10})	1.184 ± 0.039
*Mean grain size d_{50} mm	0.724 ± 0.031
Porosity	0.32
*Bulk density $g \cdot cm^{-3}$	1.78
*Organic carbon content	0.0003
*k intrinsic permeability cm^2	1.38E-10
*K hydraulic conductivity	1.29E-03

Note: * from Brusseau et al., 2002.

Table 1. Properties of the porous media (20/30-mesh Accusand) for column experiments.

Compound	Molecular Weight [g·mol^{-1}]	Solubility [mg·L^{-1}]	Density [g·cm^{-3}]
Trichloroethene (TCE)	131.39	1,200	1.462
n-Hexadecane (HEX)	226.44	Insoluble	0.770
Toluene (TOL)	92.14	535	0.867

Table 2. Chemical Properties of relevant compounds.

NAPL Scenario	Column Volume (cm^3)	NAPL Injection Direction	Residual Flush Direction	Residual Saturation [S_N] (%)	Dissolution Flush Direction
Toluene	26.8	Top Down	Bottom Up	-	Top Down
0.5:0.5 TOL:HEX	26.8	Top Down	Bottom Up	21.5	Top Down
0.2:0.8 TOL:HEX	26.8	Top Down	Bottom Up	18.0	Top Down
0.1:0.9 TOL:HEX	26.8	Top Down	Bottom Up	16.0	Top Down
0.05:0.95 TOL:HEX	26.8	Top Down	Bottom Up	23.0	Top Down
TCE	26.8	Bottom Up	Top Down	-	Bottom Up
0.5:0.5 TCE:HEX	26.8	Bottom Up	Top Down	23.8	Bottom Up
0.2:0.8 TCE:HEX	26.8	Top Down	Bottom Up	20.0	Top Down
0.1:0.9 TCE:HEX	26.8	Top Down	Bottom Up	26.4	Top Down
0.05:0.95 TCE:HEX	26.8	Top Down	Bottom Up	20.5	Top Down

Table 3. Experimental procedures for establishing NAPL and for dissolution flushing.

Sample #	Mole Fraction (TOL:HEX)	Concentration ($mg \cdot L^{-1}$)	Raoult's Law Predicted Concentration ($mg \cdot L^{-1}$)	Raoult's Law Activity Coefficient
1	0.5:0.5	407.4	267.5	1.52
3	0.2:0.8	230.6	107	2.16
4	0.1:0.9	144.4	53.5	2.70
5	0.05:0.95	100.6	26.75	3.76
6	0.01:0.99	46	5.35	8.60

Table 4. TOL:HEX static batch results and predicted Raoult's Law values. Raoult's Law activity coefficient values are calculated to show how the concentrations differed from unity ($\gamma_i^N=1$).

Sample #	Mole Fraction (TCE:HEX)	Concentration ($mg \cdot L^{-1}$)	Raoult's Law Predicted Concentration ($mg \cdot L^{-1}$)	Raoult's Law Activity Coefficient
1	0.5:0.5	634.4	600	1.06
2	0.2:0.8	275	240	1.15
3	0.1:0.9	220.5	120	1.84
4	0.05:0.95	61.4	60	1.02
5	0.01:0.99	18.76	12	1.56

Table 5. TCE:HEX static batch results and predicted Raoult's Law values. Raoult's Law activity coefficient values are calculated to show how the concentrations differed from unity ($\gamma_i^N=1$).

Mole Fraction	Toluene Dissolution Rate (s^{-1})	TCE Dissolution Rate (s^{-1})
0.5:0.5	4.00E-05	3.00E-05
0.2:0.8	5.00E-05	2.00E-05
0.1:0.9	3.00E-05	2.00E-05
0.05:0.95	2.00E-05	2.00E-05
0.01:0.99	1.00E-05	9.00E-06

Table 6. Dissolution rates for both the TOL:HEX and TCE:HEX multi-component NAPL mixtures as calculated from the time series batch experiments.

Toluene		
Mole Fraction	***Batch Activity Coefficient**	**Column Activity Coefficient**
0.5:0.5	1.52 [1.81]	1.58
0.2:0.8	2.16 [2.15]	1.46
0.1:0.9	2.70 [2.49]	1.79
0.05:0.95	3.76 [2.29]	2.30
0.01:0.99	8.60 [3.55]	NA

* values in parentheses [ ] are from time-series experiments

Table 7. Activity coefficient values for both the batch and column Toluene experiments.

TCE		
Mole Fraction	***Batch Activity Coefficient**	**Column Activity Coefficient**
0.5:0.5	1.06 [2.41]	1.32
0.2:0.8	1.15 [1.68]	1.24
0.1:0.9	1.84 [1.44]	1.27
0.05:0.95	1.02 [1.58]	3.97
0.01:0.99	1.56 [3.12]	NA

* values in parentheses [ ] are from time-series experiments

Table 8. Activity coefficient values for both the batch and column TCE experiments.

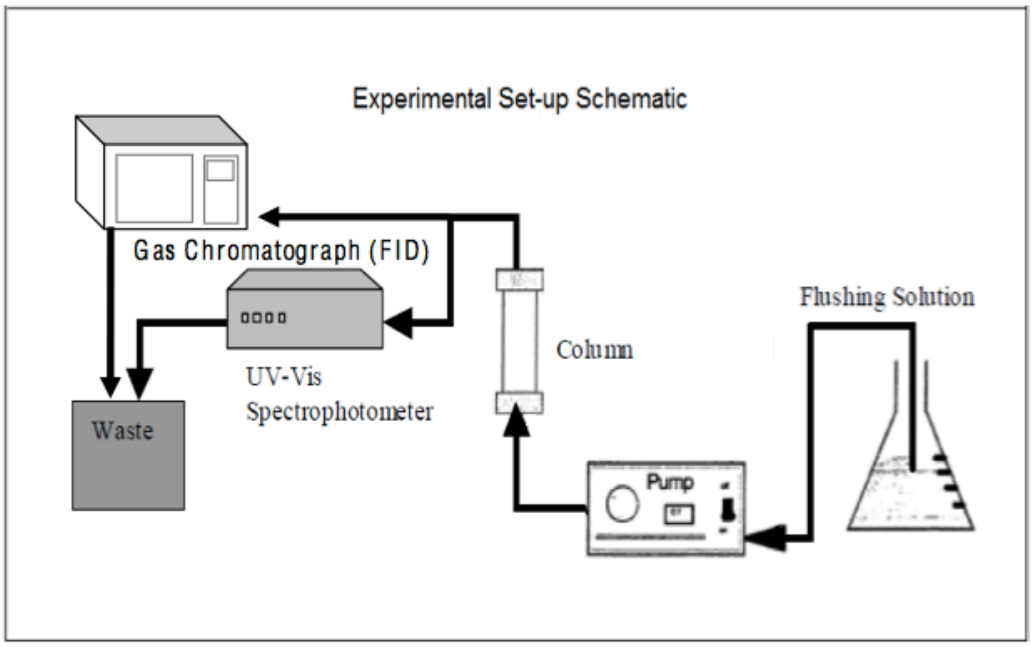

Figure 1. Schematic of Experimental Setup (adapted from Burke, 2011).

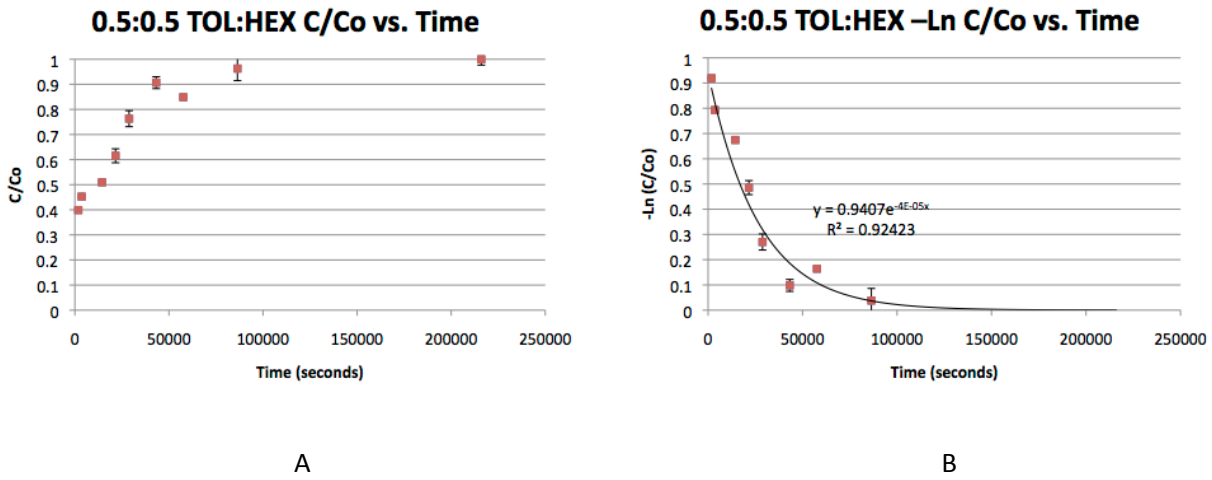

Figure 2. Dissolution rate calculation for the 0.5:0.5 TOL:HEX time series batch experiment. Graph A shows the raw data while graph B shows the natural log of the relative concentration plotted against time in order to calculate a dissolution rate.

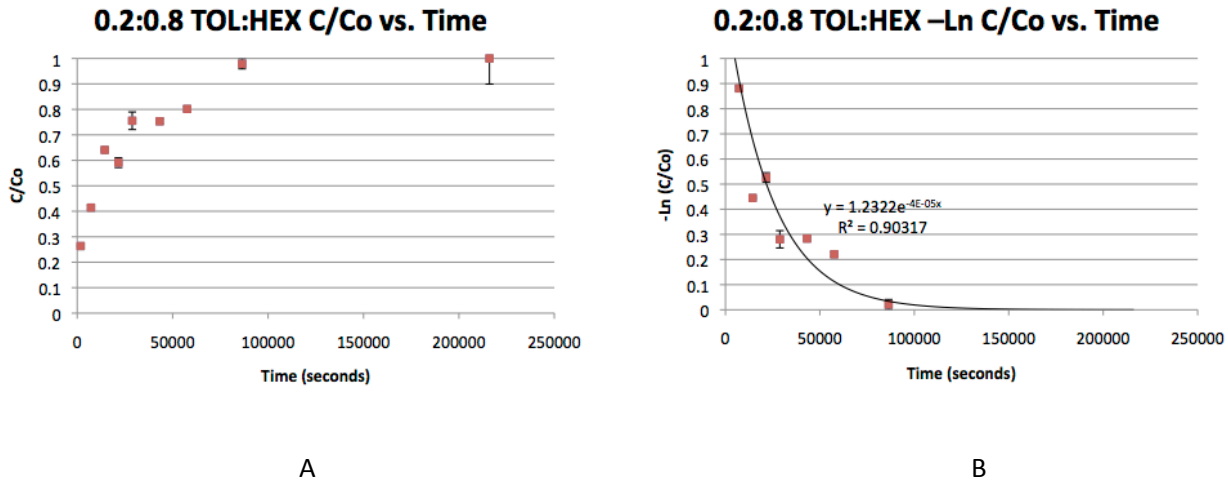

A B

Figure 3. Dissolution rate calculation for the 0.2:0.8 TOL:HEX time series batch experiment. Graph A shows the raw data while graph B shows the natural log of the relative concentration plotted against time in order to calculate a dissolution rate.

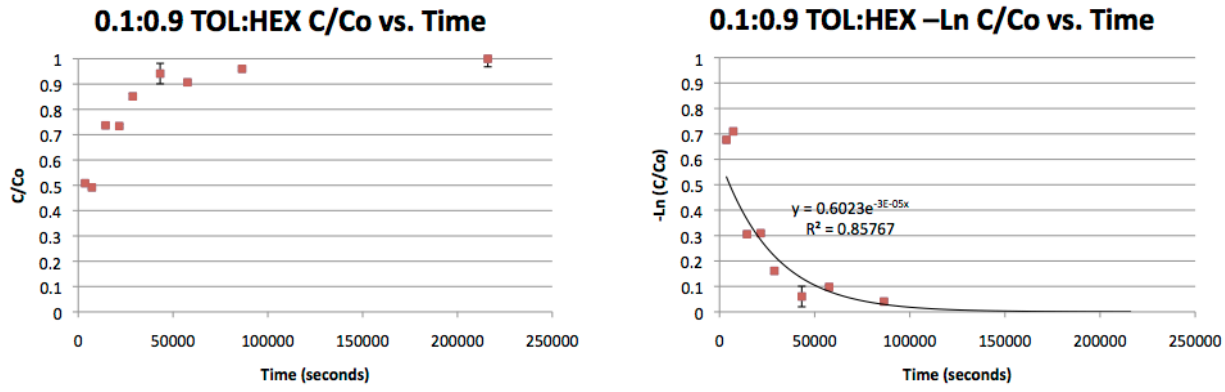

A B

Figure 4. Dissolution rate calculation for the 0.1:0.9 TOL:HEX time series batch experiment. Graph A shows the raw data while graph B shows the natural log of the relative concentration plotted against time in order to calculate a dissolution rate.

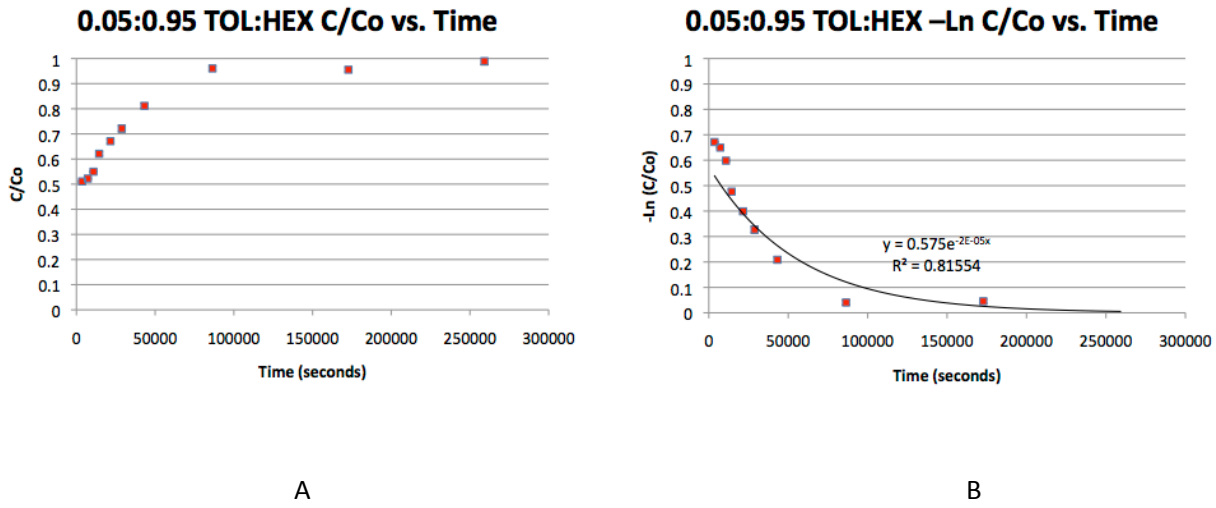

A B

Figure 5. Dissolution rate calculation for the 0.05:0.95 TOL:HEX time series batch experiment. Graph A shows the raw data while graph B shows the natural log of the relative concentration plotted against time in order to calculate a dissolution rate.

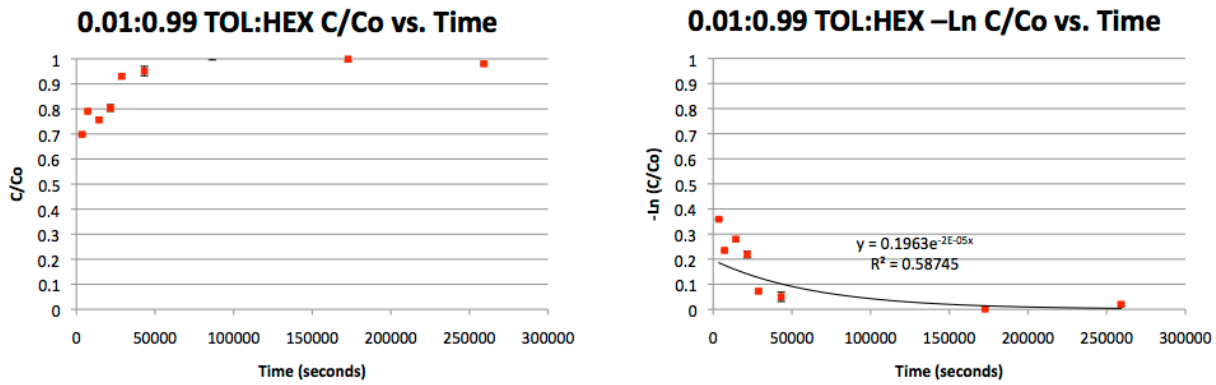

A B

Figure 6. Dissolution rate calculation for the 0.01:0.99 TOL:HEX time series batch experiment. Graph A shows the raw data while graph B shows the natural log of the relative concentration plotted against time in order to calculate a dissolution rate.

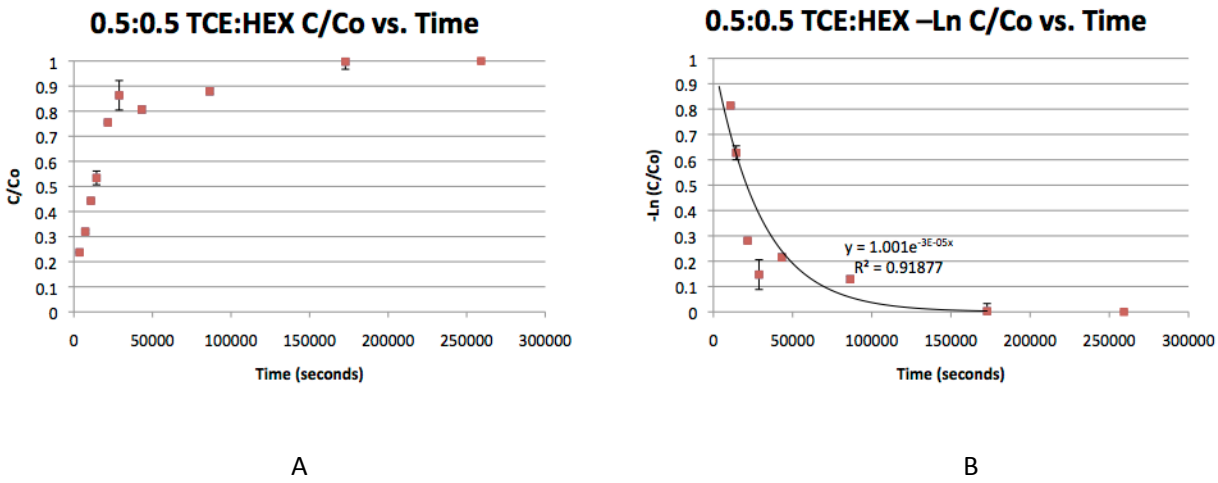

Figure 7. Dissolution rate calculation for the 0.5:0.5 TCE:HEX time series batch experiment. Graph A shows the raw data while graph B shows the natural log of the relative concentration plotted against time in order to calculate a dissolution rate.

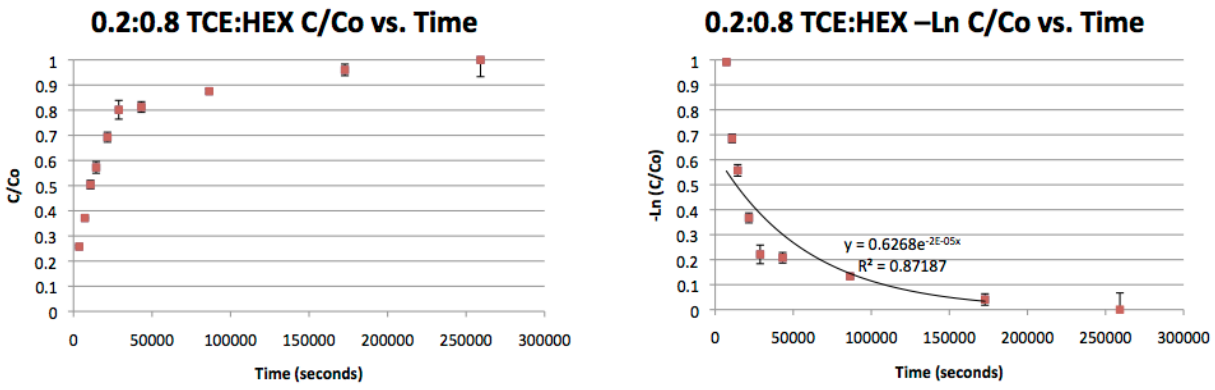

A B

Figure 8. Dissolution rate calculation for the 0.2:0.8 TCE:HEX time series batch experiment. Graph A shows the raw data while graph B shows the natural log of the relative concentration plotted against time in order to calculate a dissolution rate.

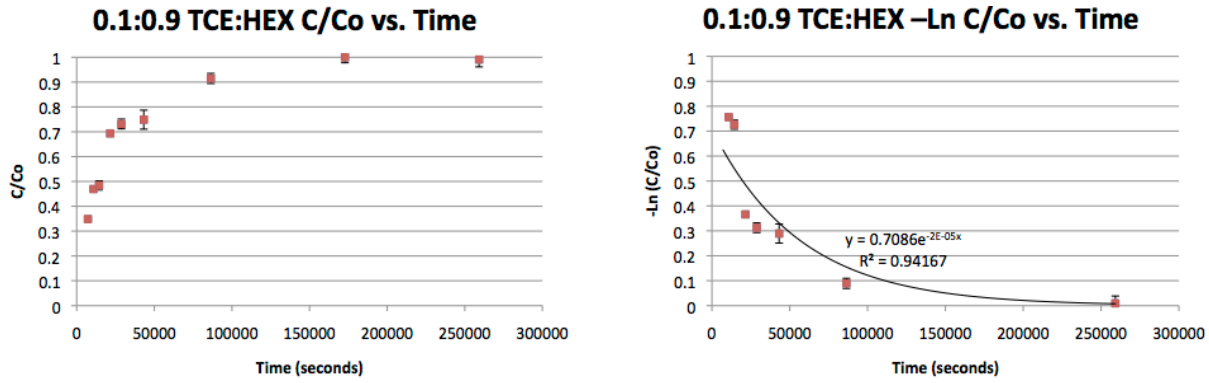

A B

Figure 9. Dissolution rate calculation for the 0.1:0.9 TCE:HEX time series batch experiment. Graph A shows the raw data while graph B shows the natural log of the relative concentration plotted against time in order to calculate a dissolution rate.

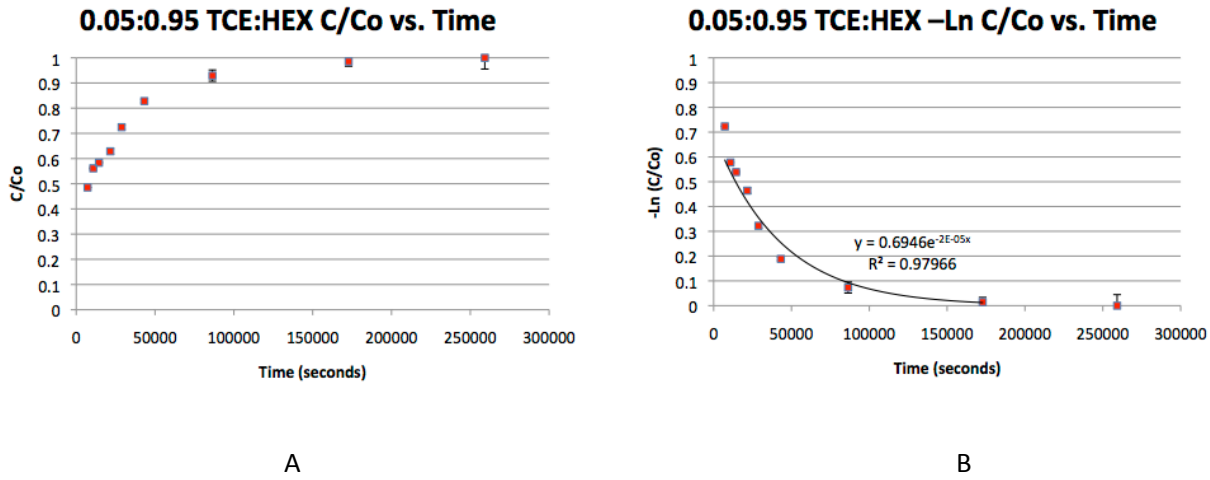

Figure 10. Dissolution rate calculation for the 0.05:0.95 TCE:HEX time series batch experiment. Graph A shows the raw data while graph B shows the natural log of the relative concentration plotted against time in order to calculate a dissolution rate.

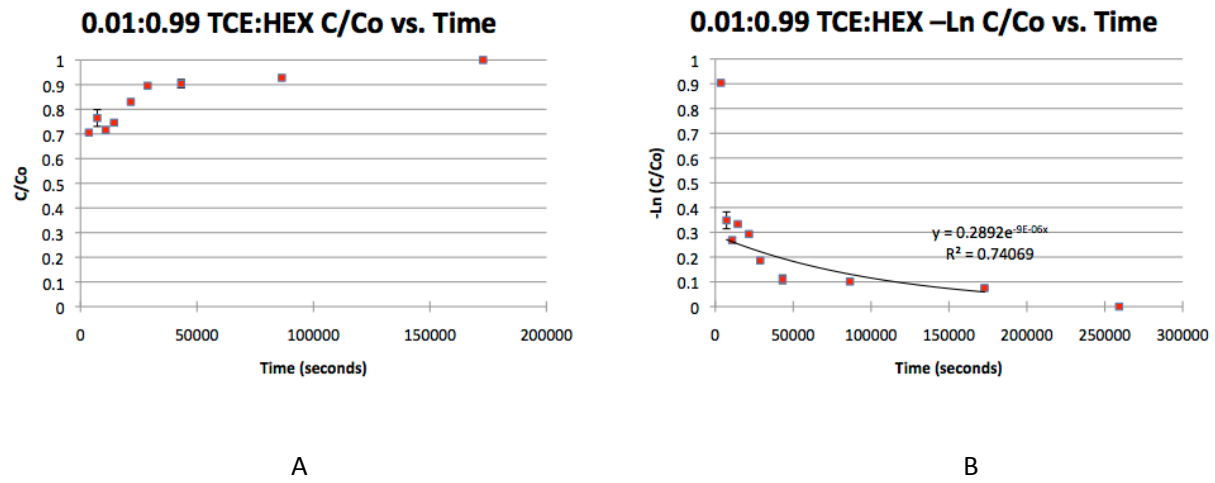

A B

Figure 11. Dissolution rate calculation for the 0.01:0.99 TCE:HEX time series batch experiment. Graph A shows the raw data while graph B shows the natural log of the relative concentration plotted against time in order to calculate a dissolution rate.

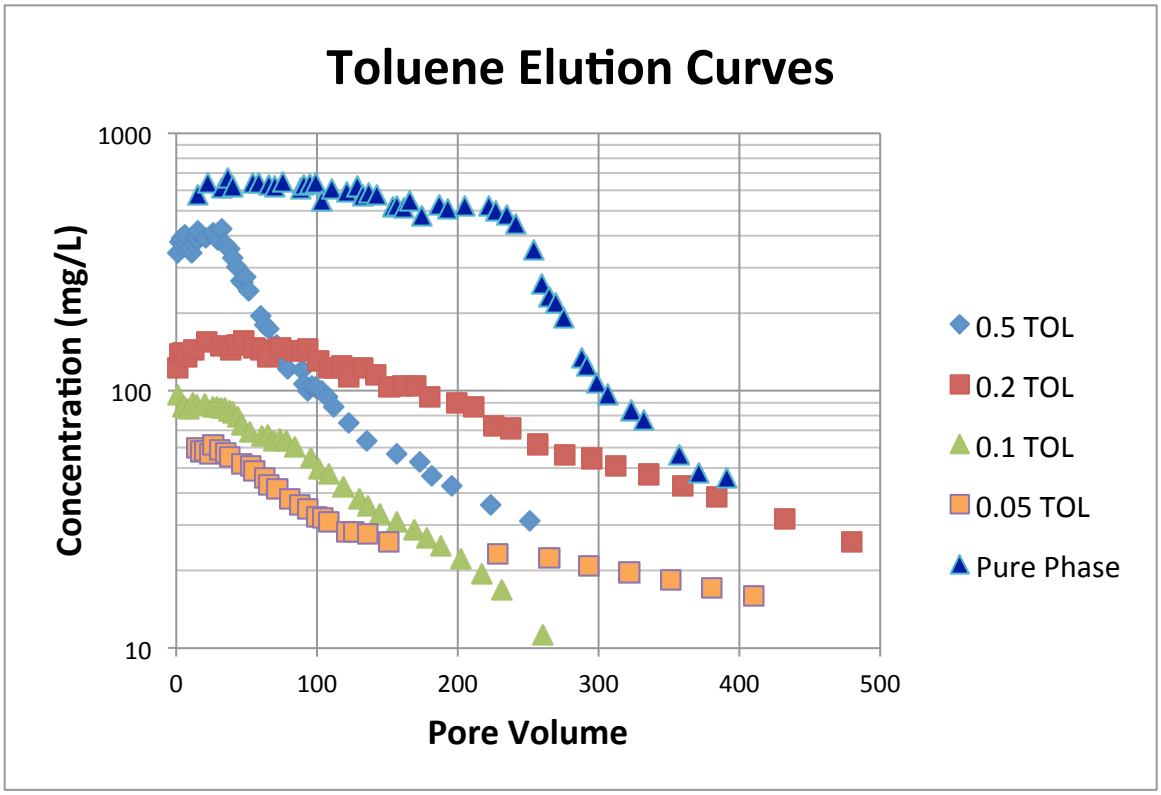

Figure 12. Toluene elution curves under uniformly packed conditions for differing mole fractions of the two-component TOL:HEX systems. Data is presented as concentrations in mgL^{-1} vs. pore volume.

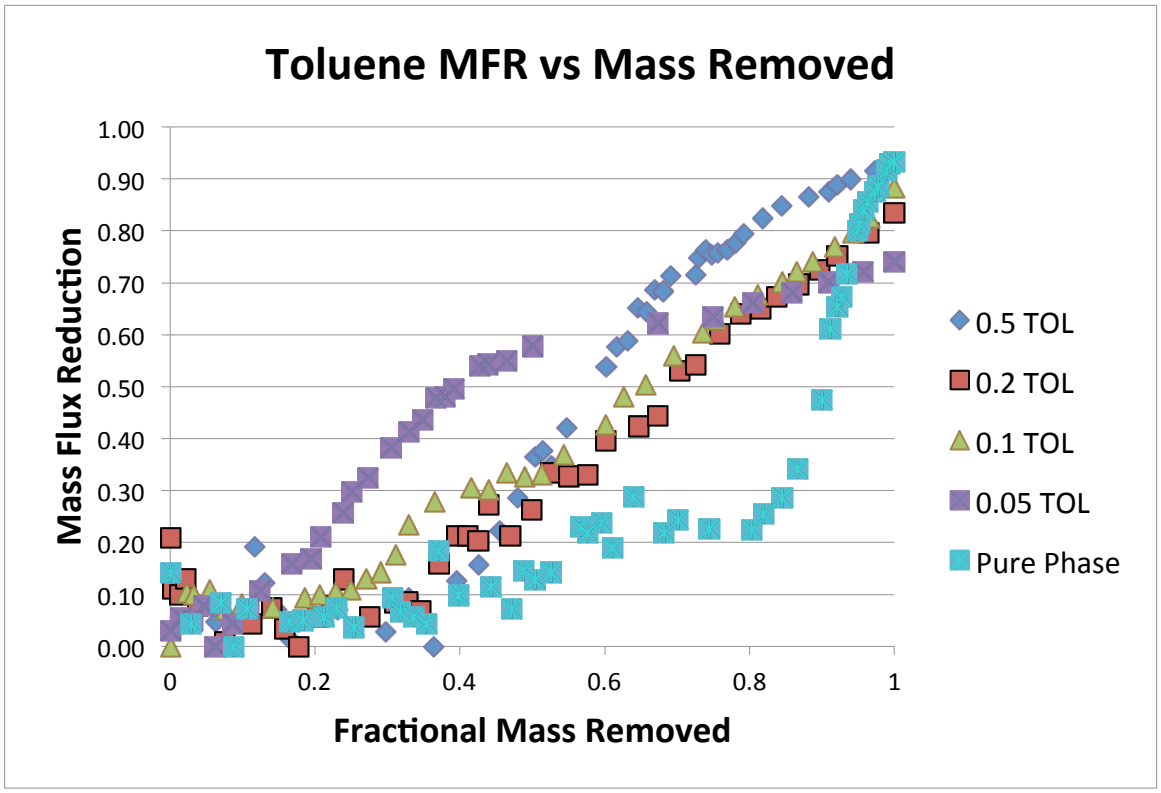

Figure 13. Toluene mass flux reduction vs. fractional mass removed for each two component TOL:HEX NAPL system. A pure phase Toluene mass flux reduction is also shown for a control.

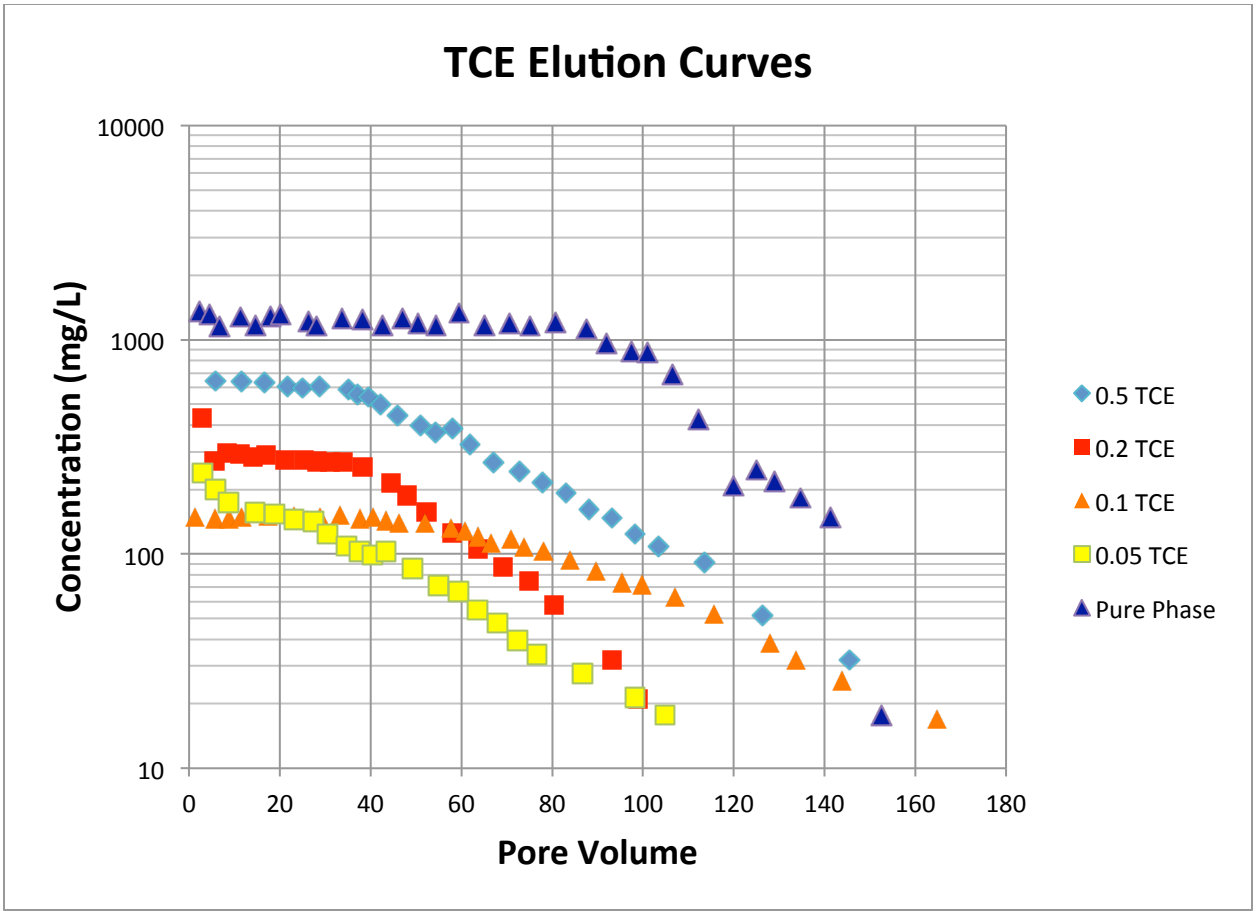

Figure 14. TCE elution curves under uniformly packed conditions for differing mole fractions of the two-component TCE:HEX systems. Data is presented as concentrations in mgL^{-1} vs. pore volume.

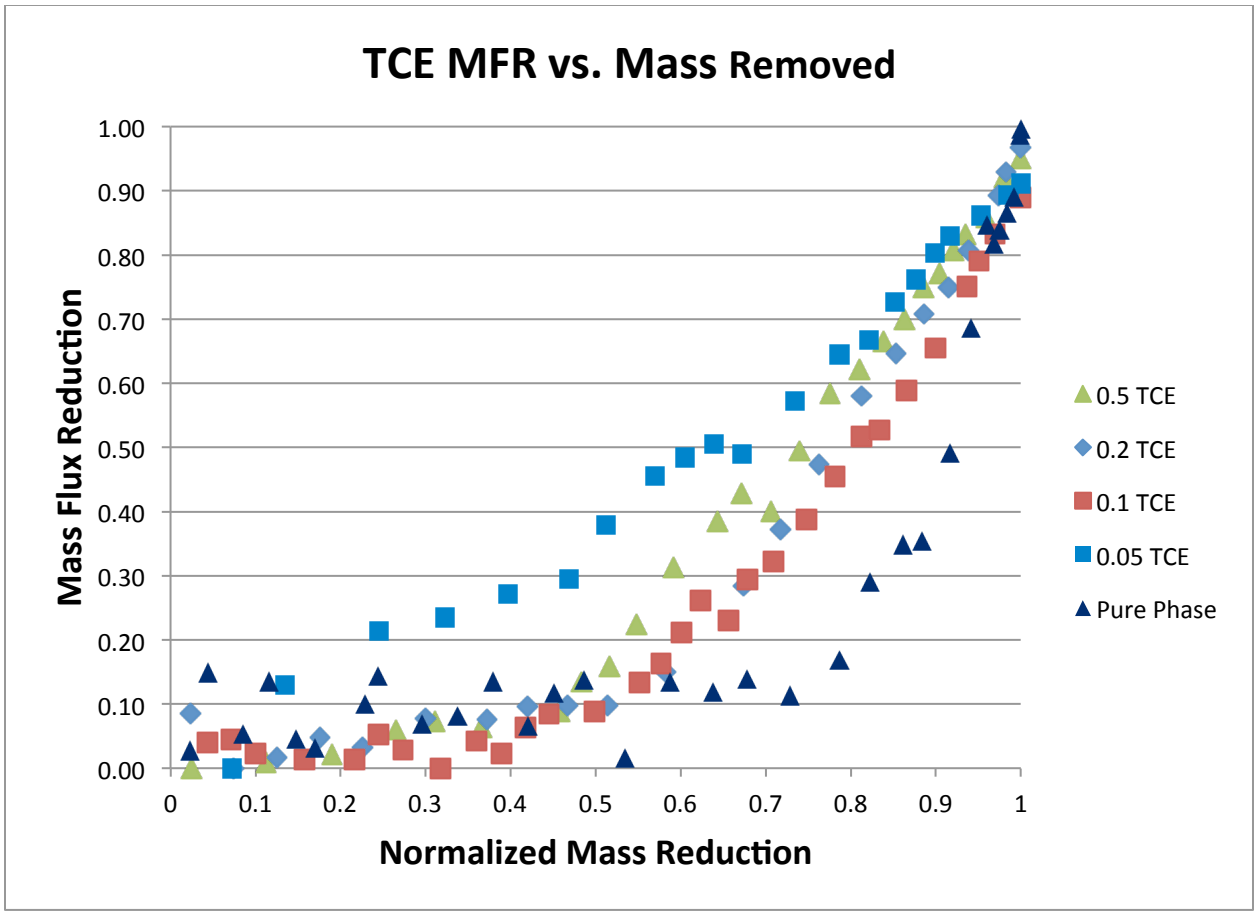

Figure 15. TCE mass flux reduction vs. fractional mass removed for each two component TCE:HEX NAPL system. A pure phase TCE mass flux reduction is also shown for a control.